

# Object-Driven Active Mapping for More Accurate Object Pose Estimation and Robotic Grasping

Yanmin Wu<sup>1</sup>, Yunzhou Zhang<sup>1,2\*</sup>, Delong Zhu<sup>3\*</sup>, Xin Chen<sup>1</sup>, Sonya Coleman<sup>4</sup>,  
Wenkai Sun<sup>2</sup>, Xinggang Hu<sup>2</sup>, Zhiqiang Deng<sup>2</sup>

**Abstract**— This paper presents the first active object mapping framework for complex robotic grasping tasks. The framework is built on an object SLAM system integrated with a simultaneous multi-object pose estimation process. Aiming to reduce the observation uncertainty on target objects and increase their pose estimation accuracy, we also design an object-driven exploration strategy to guide the object mapping process. By combining the mapping module and the exploration strategy, an accurate object map that is compatible with robotic grasping can be generated. Quantitative evaluations also show that the proposed framework has a very high mapping accuracy. Manipulation experiments, including object grasping, object placement, and the augmented reality, significantly demonstrate the effectiveness and advantages of our proposed framework.

## I. INTRODUCTION

Active mapping refers to the process of actively perceiving environments by adapting self motions of the robot based on specific criteria [1]. Active mapping has wide applications in mobile robots, e.g., unknown environment exploration and target searching [2]. In recent years, with the growing requirements on robotic manipulation in unknown or cluttered environments, active mapping also receives much attention in the manipulation community [3]–[6].

However, the output of the conventional mapping framework, e.g., ORB-SLAM2, cannot be directly used for manipulation tasks like object grasping, since the generated map does not contain object pose information. Therefore, additional processing is needed to register the object pose into the map, which is usually achieved by aligning the CAD model with object point cloud [3]–[5] or directly predicting a pose for the object using deep neural networks [4]. The problem of pose estimation for unknown objects remains unsolved. Moreover, the activeness during mapping is not sufficiently leveraged, which further limits the application of conventional mapping techniques in scenarios with high uncertainties, e.g., partially observable environments.

\*The corresponding author of this paper.

<sup>1</sup>Yanmin Wu and Xin Chen are with Faculty of Robot Science and Engineering, Northeastern University, Shenyang, China.

<sup>2</sup>Yunzhou Zhang, Wenkai Sun, Xinggang Hu, and Zhiqiang Deng are with College of Information Science and Engineering, Northeastern University, Shenyang 110819, China (Email: zhangyunzhou@mail.neu.edu.cn).

<sup>3</sup>Delong Zhu is with the Department of Electronic Engineering, The Chinese University of Hong Kong, Shatin, N.T., Hong Kong SAR, China (Email: zhudelong@link.cuhk.edu.hk).

<sup>4</sup>Sonya Coleman is with School of Computing, Engineering and Intelligent Systems, Ulster University, N. Ireland, UK.

This work was supported by National Natural Science Foundation of China (No. 61973066, 61471110) and Fundamental Research Funds for the Central Universities (N172608005, N182608004).

To address these problems, we in this paper propose an active mapping framework for robotic grasping based on our previous object SLAM [7]. The framework leverages cylinders and cubes to approximate unknown objects and fuses object pose estimation into a joint optimization process, achieving simultaneously object and camera pose estimation. We also propose an object-driven exploration strategy to actively perceive the object to eliminate the uncertainty caused by partial observation and noises of object pose estimation.

The contributions of this paper are summarized as follows:

- We extend the object pose estimation algorithm based on our previous work [7], making it more robust and accurate, suitable for robotic grasping.
- We propose an object-driven exploration strategy that takes into account the completeness of object observation and pose estimation uncertainty, which significantly improves the accuracy of the generated object map.
- To the best of our knowledge, we for the first time combine the object SLAM with an object-driven exploration strategy, achieving very accurate object mapping and complex robotic grasping. Project page <https://yanmin-wu.github.io/project/active-mapping/>

## II. RELATED WORK

### A. Active Perception and Mapping

Active perception is the process of actively adjusting sensor states by analyzing existing data to obtain more valuable information. Zhang *et al.* [8] leverage Fisher information to predict the best sensing location for reducing localization uncertainty. Zeng *et al.* [9] leverage prior knowledge between objects to establish a semantic link graph for active object searching. Zhu *et al.* [1], [10] propose to learn global topological knowledge of indoor environments using deep reinforcement learning to accelerate the efficiency of robotic exploration. Active mapping is a specific task of active perception. Charrow *et al.* [11] utilize the quadratic mutual information to guide 3D dense map building. Wang *et al.* [12] also leverage the mutual information to perform Next-Best View (NBV) selection on a sparse road map, which then serves as the semantic landmark to help accelerate the mapping process. Krieger *et al.* [13] propose a surface reconstruction method for single unknown objects. In addition to the information gain, the authors also integrate the measurement of reconstruction quality to the objective function, achieving very high accuracy and completeness.

The data-driven exploration strategy proposed in this work is implemented based on the information entropy but additionally integrates the requirement for accurate object pose estimation. Another major difference with other methods is that the output of our proposed method is an object map that is compatible with complex grasping tasks.

### B. Object Map for Grasping

An object map is an indispensable module for complex grasping tasks, e.g., object placement and arrangement. Wada *et al.* [3] propose to reconstruct objects by incremental object-level voxel mapping. The object pose is initialized by voxel points, but there is a large error in scale. The ICP algorithm then is used to align the initialized object with the CAD model to further optimize the pose, the performance of which highly depends on the registration accuracy of the CAD model. Sucar *et al.* [4] propose a multi-category object descriptor and a probabilistic rendering model to infer object poses and shapes. The target object is regarded as a landmark in SLAM and is involved in the joint optimization to help generate an accurate object map. The major deficiency of this method is that the model requires a tedious category-level training process for each object. Labbé *et al.* [5] propose a single-view 6-DoF object pose estimation method and utilize the object-level bundle adjustment in the SLAM framework to optimize the object map. However, their proposed method is only targeted for known objects. Almeida *et al.* [6] leverage the SLAM framework to densely map unknown objects for accurate grasping point detection, but the object pose is not estimated.

We also use the SLAM framework to generate the object map used for complicated grasping tasks. However, unlike previous studies, we focus on the pose estimation of unknown objects in the environment and leverage active mapping techniques to generate a more accurate and complete object map. To the best of our knowledge, this is the first work that applies active mapping to object pose estimation and unknown object grasping.

### III. SYSTEM OVERVIEW

An overview of the proposed system is presented in Fig. 1, which forms a closed-loop for incrementally exploring and mapping the desk environment. Specifically, the motion module is used to control the robot to execute observation commands. The perception module is used to estimate camera pose and build the point cloud map, and most importantly, extract objects from the map and estimate their poses. The output of this module is an object map with 9-DoF object pose registered, which can help the robot to perform tasks like motion planning and object manipulation. The analysis module measures object uncertainty and predicts the information gain of different camera views. The view with the largest information gain is selected as the NBV and passed to the motion module to enable active exploration. This work aims to incrementally build a global object map with the minimum effort and the maximum accuracy for robotic grasping.

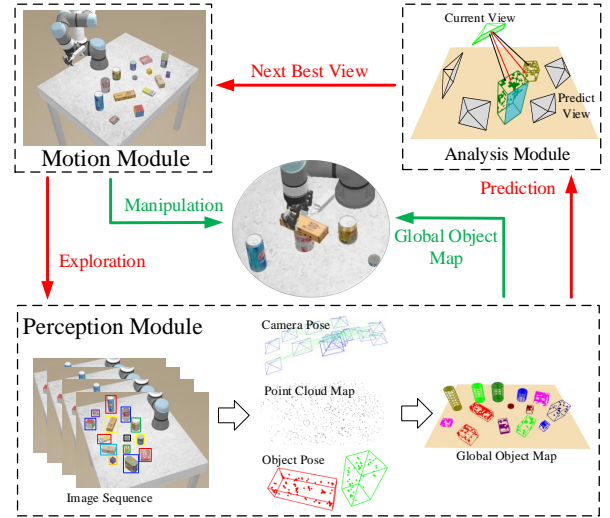


Fig. 1: The proposed system framework.

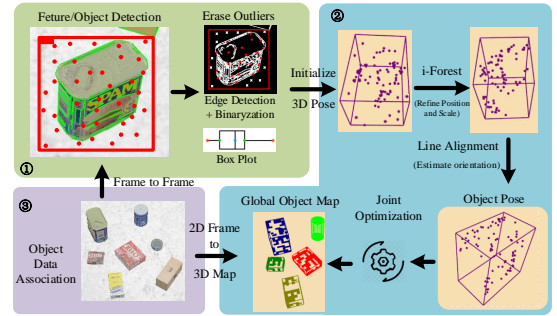


Fig. 2: The framework of object pose estimation.

### IV. OBJECT DRIVEN ACTIVE MAPPING

#### A. Object Map Building

The goal of object association and pose estimation is to identify the same objects from different camera views and then estimate their poses w.r.t. the global frame. Accurate object association and pose estimation is the key to enabling successful grasping with the presence of multi objects. Here, we briefly present our previous work [7], which implements an object SLAM system based on a robust object association algorithm.

As demonstrated in Fig. 2, the point-line features and objects are first detected on each image frame. After filtering out the background points for each object, the remaining points are aggregated into the corresponding object point cloud in the global map. The correspondence is found by a robust object association algorithm in [7]. We then fit a tight 3D cube for the object point cloud based on the i-Forest and line alignment to initialize the object pose. Then, a joint optimization between the camera and object pose is conducted to further improve the pose estimation accuracy. In this work, we propose a new optimization algorithm that can achieve highly accurate object pose estimation.

The object pose is parameterized with  $O = \{t, \theta, s\}$ , which represents the translation, orientation, and scale of the object, respectively. The error function used to optimize the

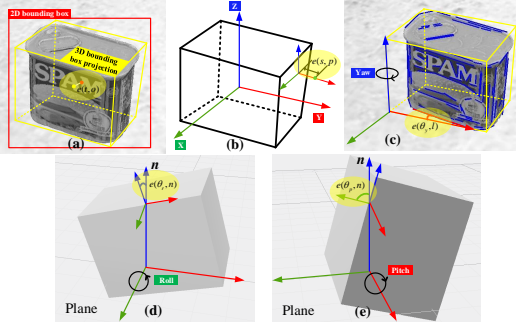


Fig. 3: Error definition of object pose optimization.

object pose is formulated as follows,

$$\arg \min_{\mathbf{o}} \sum (e(\mathbf{t}, \mathbf{o}) + e(\mathbf{s}, \mathbf{p}) + e(\theta_y, l) + e((\theta_r, \theta_p), \mathbf{n})), \quad (1)$$

which is then solved by nonlinear optimizers, e.g., the Levenberg-Marquardt method.

The first item in Eq. (1) is a position error. As shown in Fig. 3(a), the 3D center  $\mathbf{s}$  of the object is projected onto the image plane, and the distance between the projected point and the center of 2D bounding box is taken as the first error,

$$e(\mathbf{t}, \mathbf{o}) = \|\pi(T_c^{-1}\mathbf{t}) - \mathbf{o}\|_2, \quad (2)$$

where  $\pi$  is the projection matrix,  $T_c$  is the camera pose.

The second item is a scale error. As shown in Fig. 3(b), similar to the idea of CubeSLAM [14], the 3D object points  $\mathbf{p}$  should be constrained inside the 3D cube, hence the distance from the point  $\mathbf{p}$  to the corresponding cube surface is taken as the error,

$$e(\mathbf{s}, \mathbf{p}) = \max(|T_o^{-1}\mathbf{p}| - \mathbf{s}, 0), \quad (3)$$

where  $T_o$  is the object pose.

The third item is the error between the yaw  $\theta_y$  of the object and the direction  $\theta_l$  of line  $l$  in the image, shown in Fig. 3(c). The direction of the object should be parallel with the detected lines, and thus the angle should be minimized,

$$e(\theta_y, l) = \|\theta_y - \theta_l\|_2. \quad (4)$$

The fourth item is the roll and pitch error, shown in Fig. 3(d) and (e). For the grasping task, objects are placed flat on the desktop, the normal vector  $\mathbf{n}$  of which can be obtained by a RANSAC-based plane fitting algorithm. The pitch of the object should be perpendicular to  $\mathbf{n}$ , while the roll should be parallel with  $\mathbf{n}$ ,

$$\begin{aligned} e(\theta_r, \mathbf{n}) &= \|\theta_n - \theta_r\|_2, \\ e(\theta_p, \mathbf{n}) &= \|(\theta_n - \theta_p) - 90^\circ\|_2. \end{aligned} \quad (5)$$

By replacing the joint optimization module in Fig. 2 with the new optimization algorithm, the accuracy of object pose estimation can be further improved.

### B. Observation Completeness Measurement

The incompleteness of map building provides the driving force for active exploration. Existing studies usually take the entire environment as the exploration target [11], [15] or focus on reconstructing a single object [13], [16], which

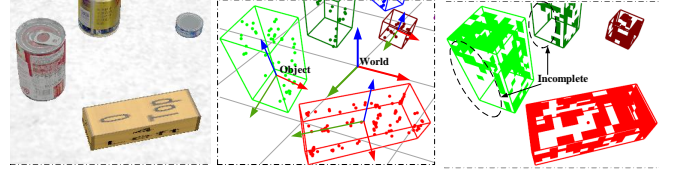


Fig. 4: Illustration of observation completeness measurement. Left: Raw image. Center: Objects with point cloud. Right: Objects with surface grids.

is not suitable for building the object map required by robotic grasping. The reasons are as follows: 1) The insignificant or unimportant regions in the environment will interfere with the decisions made for exploration and misguide the robot into the non-object area; 2) it will significantly increase the computational cost and thus reduce the efficiency of the whole system. In this work, we propose an object-driven active exploration strategy for building the object map incrementally. The strategy is designed based on observation completeness of the object, which is defined as follows.

As demonstrated in Fig. 4, the point cloud of an object is first transformed from the world frame to the object frame, and then is projected onto the five surfaces of the estimated 3D cube. Here, the bottom face is not considered. Each of the five surfaces is discretized into a surface occupancy grid map [17], [18] with  $m * m$  resolution ( $m = 1\text{cm}$  in our implementation). Each grid cell can have one of the following three statuses:

- **unknown**: the grid is not observed by the camera;
- **occupied**: the grid is occupied by the point clouds;
- **free**: the grid can be seen by the camera but is not occupied by the point clouds.

Based on the occupancy grid map, we leverage information entropy to measure observation completeness. The entropy of each grid cell is defined by a binary entropy function:

$$H_{grid}(p) = -p \log(p) - (1 - p) \log(1 - p), \quad (6)$$

where  $p$  is the probability of a grid cell being occupied and its initial value before exploration is set to 0.5. The total entropy is then defined as

$$H_{obj} = \sum_{o \in \mathbb{O}} H_o + \sum_{f \in \mathbb{F}} H_f + \sum_{u \in \mathbb{U}} H_u, \quad (7)$$

and the normalized total entropy is

$$\bar{H}_{obj} = H_{obj} / (|\mathbb{O}| + |\mathbb{F}| + |\mathbb{U}|), \quad (8)$$

where  $\mathbb{O}, \mathbb{F}, \mathbb{U}$  are sets of the occupied, free, and unknown grid cells, respectively.  $|\mathbb{X}|$  represents the size of  $\mathbb{X}$ . As objects continue to be explored, the number of unknown grid cells is gradually reduced, making  $\bar{H}_{grid}$  a smaller value. The lower the  $\bar{H}_{grid}$  is, the higher the observation completeness is. NBV is then defined as the view that minimizes  $\bar{H}_{grid}$ .

Additionally, based on the definition of the surface grid, an outlier removal method is also implemented, which is added after the i-Forest algorithm in Fig. 2. The idea is illustrated in Fig. 5. The 3D cube is first divided into slices in one of the

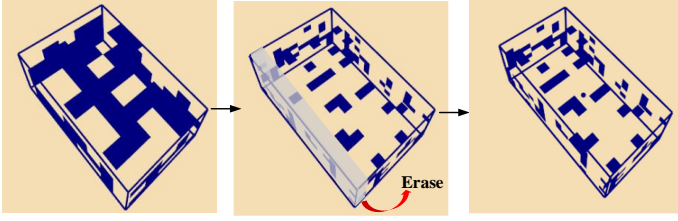


Fig. 5: Pose refinement based on surface grid sparsity.

axes, and then the number of occupied grid cells in each slice ( $n_0, n_1, \dots, n_K$ ) is counted. Edge slices, e.g., slice 0 and  $K$ , that satisfy  $n_i < 1/3n_{i+1}$  ( $0 < i < K/2$ ) or  $n_i < 1/3n_{i-1}$  ( $K/2 < i < k$ ) are not considered during object pose estimation, i.e., Eq. (1). Such processing is conducted on all three axes. This method actually shares some similarities with the i-Forest algorithm but shows better performance in grouped outlier removal, which is hard to identify by the i-Forest method.

### C. Object-Driven Exploration

**Information Gain Definition:** Object-driven exploration aims to predict the information gain of different camera views and then select the one that can maximize the information gain, i.e., the NBV, to explore, as shown in Fig. 6(b). The information in this work is defined as the map uncertainty and accuracy. The information gain is thus defined as the measurement of uncertainty reduction and accuracy improvement after the camera is placed at a specific pose. Conventionally, information gain is defined based on the area of unknown regions in the environment, i.e., the black holds in Fig. 6(a), which cannot effectively guide the object map building, as mentioned in Section IV-B. Compared with the conventional one, our proposed information gain is built on the observation completeness measurement, shown in the right figure of Fig. 6(a), and incorporates the influence on object pose estimation, which is one of the key contributions in this work.

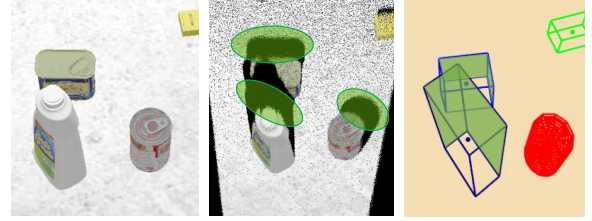
**Information Gain Modeling:** As indicated by the definition, information gain is related to many factors. We thus first manually design a feature vector to parameterize the factors, and then define a utility function to model the information gain. The feature vector used for characterizing an object  $\mathbf{x}$  is designed as follows,

$$\mathbf{x} = (H_{obj}, \bar{H}_{obj}, R_o, R_{IoU}, \bar{V}_{obj}, s), \quad (9)$$

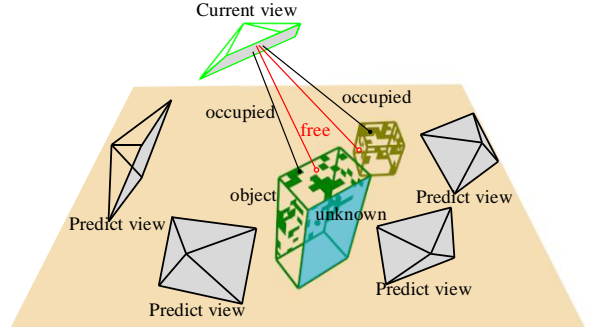
where  $H_{obj}$ , and  $\bar{H}_{obj}$  are defined by Eq. (6) - (8),  $R_o$  is the ratio of occupied grids to the total grids of the object, which indicates the richness of its surface texture,  $R_{IoU}$  is the 2D mean IoU with adjacent objects used for modeling occlusion under a specific camera view,  $\bar{V}_{obj}$  is the current volume of the object, and  $s$  is a binary value used for indicating whether the object is fully explored.

The utility function for NBV selection then is defined as,

$$f = \sum_{\mathbf{x} \in I} ((1 - R_o)H_{obj} + \lambda(H_{IoU} + H_V)) s(\mathbf{x}), \quad (10)$$



(a) Different definitions of information gain in exploration.



(b) Information gain under different camera views.

Fig. 6: Demonstration of the object-driven exploration.

where  $I$  is the predict camera view,  $\lambda$  is a weight coefficient ( $\lambda = 0.2$  in our implementation), and  $H_{IoU}, H_V$  share the same formula,

$$H = -p \log(p). \quad (11)$$

The first item  $\sum_{\mathbf{x} \in I} (1 - R_o)H_{obj}$  in Eq. (10) is used to model the total weighted uncertainty of the object map under the predict camera view. Here we give more weight not only to the unknown grids but also the free ones by using  $1 - R_o$ . The reason is that we want to encourage more explorations in free regions to find more image features that are neglected by previous sensing.

The second item  $\sum_{\mathbf{x} \in I} H_{IoU}$  in Eq. (10) defines the uncertainty on object detection, which is one of the key factors affecting object pose estimation (see Fig. 2). The uncertainty is essentially caused by occlusions between objects. We use this item to encourage a full observation of the object. The variable in Eq. (11) is the rescaled 2D IoU, i.e.,  $p = R_{IoU}/2$ .

The third item  $\sum_{\mathbf{x} \in I} H_V$  in Eq. (10) models the uncertainty on object pose estimation. Under different camera views, the estimated object poses are usually different, and consequently, induce the changes in object volume. Here, we first fit a standard normal distribution using the normalized history volumes  $\{\bar{V}_{obj}^{(0)}, \bar{V}_{obj}^{(1)}, \dots, \bar{V}_{obj}^{(t)}\}$  of each object, and then take the probability density of  $\bar{V}_{obj}^{(t)}$  as the  $p$  value in Eq. (11). This item essentially encourages the camera view that can converge the pose estimation process.

The  $s(\mathbf{x})$  in Eq. (10) indicates whether the object should be considered during the calculation of the utility function.  $s(\mathbf{x})=0$ , if the following condition is satisfied:  $(\bar{H}_{grid} < 0.5 \vee R_o > 0.5) \wedge p(\bar{V}_{obj}^{(t)}) > 0.8$ . If this condition holds for all the objects, or the maximum tries is achieved (10 in this work), the exploration will be finished.



TABLE I: ACCURACY OF OBJECT POSE ESTIMATION.

Scene	Metrics	Ours	Random.	Cover.	Init.
1	3D IoU	<b>0.427</b>	0.3056	0.3329	0.3586
	2D IoU	<b>0.6225</b>	0.4571	0.5221	0.5212
	CDE	<b>1.5272</b>	2.2699	1.7876	2.2022
	YAE	3.5	4.8	3.8	<b>2.8</b>
2	3D IoU	<b>0.4307</b>	0.3017	0.4224	0.3400
	2D IoU	<b>0.8679</b>	0.6422	0.7730	0.6480
	CDE	<b>1.4646</b>	2.1096	1.5931	1.9822
	YAE	2.4	<b>1.8</b>	2.7	2.4
3	3D IoU	<b>0.4132</b>	0.3125	0.3685	0.2617
	2D IoU	<b>0.6225</b>	0.4915	0.5517	0.3909
	CDE	1.5503	2.0672	<b>1.4841</b>	2.7489
	YAE	3.9	<b>3.7</b>	3.8	4.9
4	3D IoU	<b>0.4790</b>	0.3824	0.3664	0.3007
	2D IoU	<b>0.6536</b>	0.5886	0.4788	0.4869
	CDE	<b>1.3335</b>	1.3514	1.7508	1.927
	YAE	2.9	2.8	<b>2.1</b>	<b>2.1</b>
5	3D IoU	<b>0.5177</b>	0.2696	0.2884	0.3720
	2D IoU	<b>0.6263</b>	0.4297	0.4326	0.6142
	CDE	<b>1.3704</b>	2.5077	2.1753	2.0084
	YAE	3.9	<b>2.1</b>	3.9	<b>2.1</b>
6	3D IoU	<b>0.4411</b>	0.3000	0.3597	0.2916
	2D IoU	<b>0.5437</b>	0.4850	0.4783	0.5042
	CDE	<b>2.5998</b>	3.4278	2.8411	3.4965
	YAE	<b>2.3</b>	2.7	3	2.7
7	3D IoU	<b>0.4626</b>	0.2118	0.4133	0.3153
	2D IoU	<b>0.6017</b>	0.3839	0.5569	0.4541
	CDE	1.49928	2.3822	<b>1.4832</b>	2.0467
	YAE	<b>2.1</b>	4.5	2.5	2.5
Mean	3D IoU	<b>0.453</b>	0.2977	0.3645	0.3200
	2D IoU	<b>0.6483</b>	0.4969	0.5419	0.5171
	CDE	<b>1.6207</b>	2.3022	1.8736	2.3446
	YAE	3	3.2	3.1	<b>2.8</b>

Based on the utility function, the NBV is continuously selected and leveraged to guide the exploration process, during which the global object map is also incrementally built up, as indicated in Fig. 1.

## V. EXPERIMENTAL RESULTS

To verify the effectiveness of the proposed framework, we set up a robotic grasping scene in the Sapine simulator, shown in Fig. 8, the number of objects and the scene complexities vary in different scenes.

### A. Evaluation of Object Pose Estimation

Accurate pose estimation for objects is the key to ensure successful robotic grasping. To quantitatively evaluate the influence of active exploration on object pose estimation, we compare our object-driven method with two commonly used baseline strategies, i.e., randomized exploration and coverage exploration. As indicated in Fig. 8, for randomized exploration, the camera pose is randomly sampled from the reachable set relative to the manipulator, while for coverage exploration, a coverage trajectory based on Boustrophedon

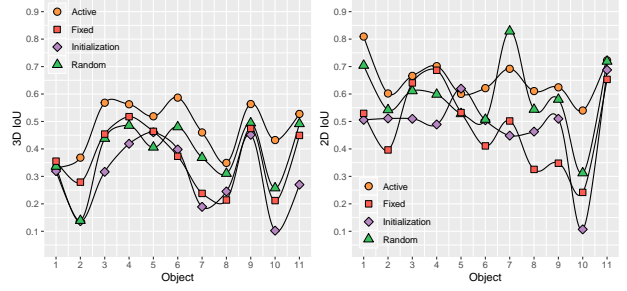


Fig. 7: 3D IoU and 2D IoU estimated by different methods.

decomposition is leveraged to scan the scene. At the beginning of all the explorations, an initialization step, in which the camera is sequentially placed over the four desk corners from a top view, is applied to start the object mapping process. The simulator provides the ground truth of object position, orientation, and size. Correspondingly, the accuracy of pose estimation is evaluated by the Center Distance Error (CDE, cm), the Yaw Angle Error (YAE, degree), and the IoU (including 2D IoU from the top view and 3D IoU) between the ground truth and our estimated results.

Table I shows the evaluation results in seven scenes (Fig. 8). We can see our proposed object-driven exploration strategy achieves a 3D IoU of 45.3%, which is 15.53%, 8.85%, and 13.3% higher than that of the randomized exploration, the coverage exploration, and the initialization, respectively. For 2D IoU, our method achieves an accuracy of 64.83%, which is 15.14%, 10.64%, and 13.12% higher than the baseline methods and initialization, respectively. In terms of CDE, our method reaches 1.62cm, significantly less than other methods. For YAE, all exploration strategies achieve an error of approximately  $3^\circ$ , which verifies the robustness of our line-alignment based yaw angle optimization method in Eq. (4)-(5). Moreover, we also find that randomized exploration sometimes performs worse than the initialization result (row 2, 5, and 7), indicating that increasing observations not necessarily results in more accurate pose estimation, and purposeful exploration is necessary.

Fig. 7 shows the position estimation results of 11 objects in Fig. 8(d), in which the 2D IoU from the top view and the 3D IoU are reported. It can be seen that our proposed strategy achieves higher 3D IoU and 2D IoU scores compared with the baseline methods.

### B. Evaluation of Object Map Quality

The mapping results are demonstrated in Fig. 8. The cubes and cylinders are used to model the objects, including poses and scales, based on their semantic categories. We can see that the system can accurately model different objects, as the number of objects is increased, shown in Fig. 8(a)-(e), which demonstrates its robustness. In Fig. 8(f)-(h), we demonstrate some behaviors exhibited by our object-driven exploration strategy. 1) Among objects with various sizes, our method focuses more on large objects with lower observation completeness (see Fig. 8(f)). 2) When the objects are placed unevenly, our proposed strategy can quickly concentrate the camera on object regions, thus avoiding unnecessary and

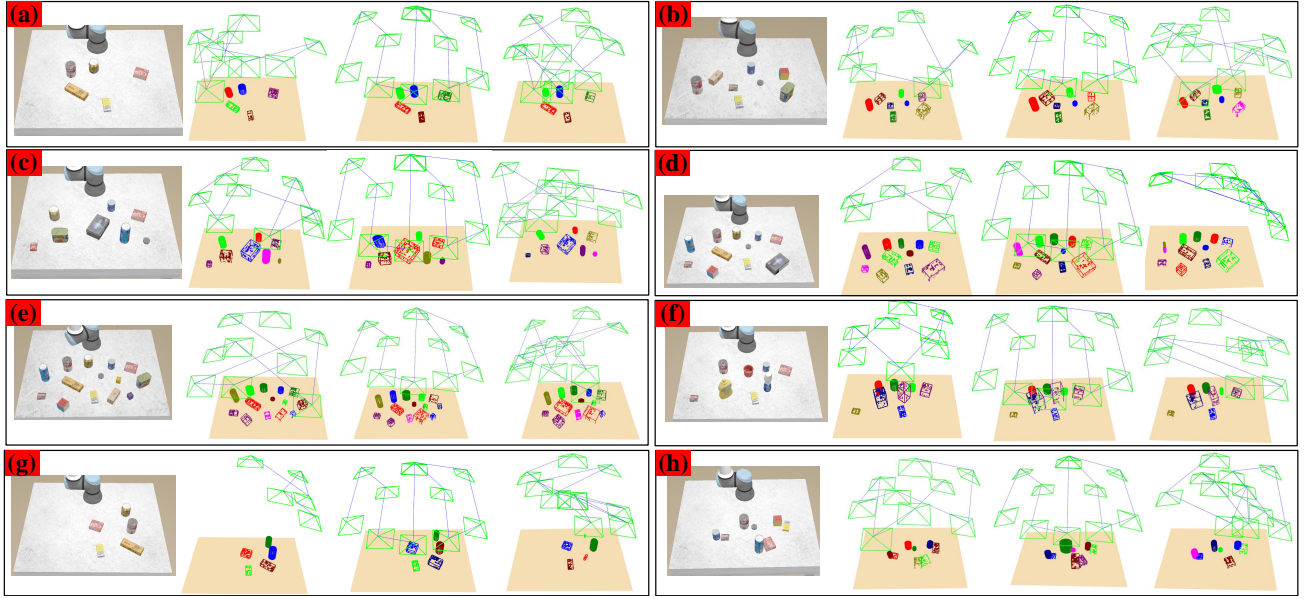


Fig. 8: Comparison of mapping results. The first column in the sub-picture: the scene image; the second column: the result of our object-driven exploration; the third column: the result of the coverage exploration; the fourth column: the result of the randomized exploration.

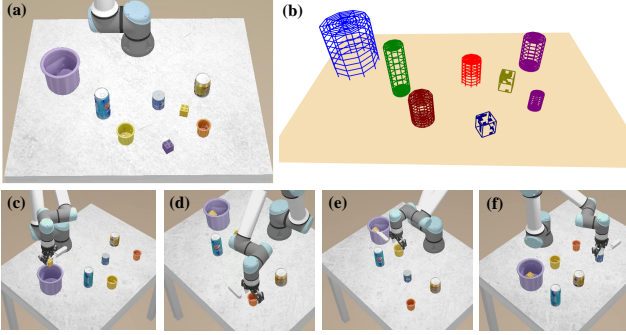


Fig. 9: Object placement according to the global object map.

time-consuming exploration (see Fig. 8(g)). 3) For scenes with objects close to each other, our method can place more attention on regions with less occlusions (see Fig. 8(h)). These behaviors verify the effectiveness of our exploration strategy. It can also be seen that our method has a shorter exploration path, which demonstrates its efficiency.

### C. Object Grasping Experiment

In this experiment, we leverage the incrementally generated object map to perform object grasping. Fig. 11 demonstrates the grasping of objects in Fig. 8(e). It is found that the center and direction of the objects have a great influence on grasping performance. Our proposed method performs well in terms of these two metrics, thus ensuring high-quality grasping. From the experiments, we find grasping failure is mainly caused by the measurement error of object height. This is because the robot tends to observe objects from the top view, which is susceptible to errors in depth. This is also the reason why 2D IoU is generally higher than 3D IoU, implying the necessity of multi-angle exploration. Overall, our pose estimation results can meet the requirements of object grasping.

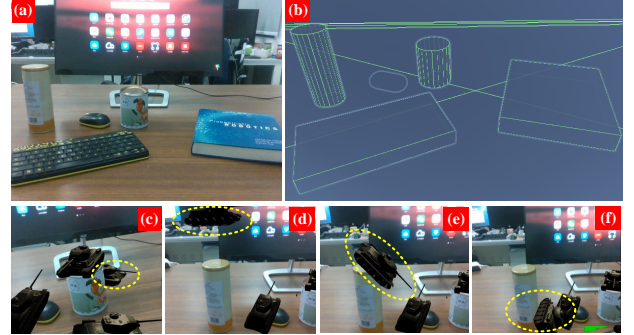


Fig. 10: Demonstration of the occlusion and collision effects.

### D. Object Placement Experiment

The global object map can help the robot to perceive the global environment rather than a single object, enabling it to make more intelligent decisions. To verify the global perception capabilities introduced by object mapping, we design the object placement experiments. As shown in Fig. 9(a), the robot is required to put the blocks into a big cup and then sort other objects according to their sizes.

The global object map is shown in Fig. 9(b), which contains the semantic labels, size, and pose of the objects. The robot grasps the object according to its pose, and places it based on the size and height of the object (Fig. 9 (c)-(f)).

### E. Augmented Reality Experiment

Augmented reality is one of the most important applications of object mapping, which can provide more complete environment information for augmented reality, thus a more realistic immersive experience can be achieved. Here, we add virtual objects in Fig. 10(a) to extend the proposed method in this work and further verify the effectiveness of pose estimation.

From the experimental results, the desktop scene is first

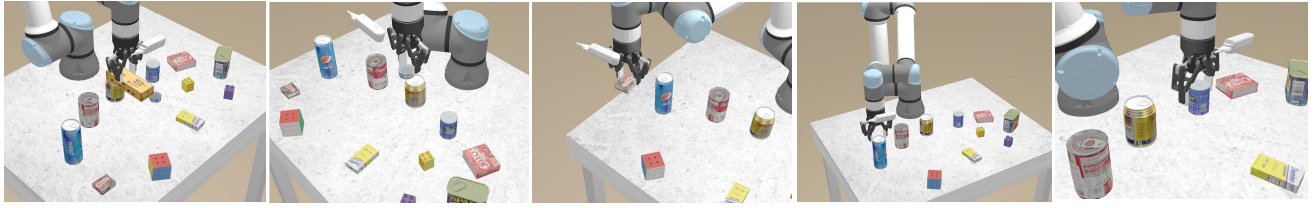


Fig. 11: The demonstration of grasping process.

modeled, and an object-level map is then obtained (see Fig. 10(b)). Fig. 10(c) demonstrates the occlusion effect, in which the virtual tank behind the cup is partially observed, and the tank above the cup can still be fixed in space. Fig. 10(d)–(f) show the collision effect, in which the tank falls and collides with the cup, and finally drops on the desktop.

## VI. CONCLUSION

In this paper, we for the first time present an object-driven active object mapping framework. The framework aims to enable the full observation and accurate pose estimation of unknown objects, and then implement complex robotic grasping. Extensive experiments significantly verify the effectiveness of our proposed framework. The presented idea and methods in this work will significantly push forward related studies in this research area. The major limitation of this work lies in that the framework currently cannot model complex objects that have irregular shapes, which is also the focus of our next-step research.

## REFERENCES

- [1] D. Zhu, T. Li, D. Ho, C. Wang, and M. Q.-H. Meng, "Deep reinforcement learning supervised autonomous exploration in office environments," in *2018 IEEE International Conference on Robotics and Automation (ICRA)*. IEEE, 2018, pp. 7548–7555.
- [2] D. Zhu, Y. Du, Y. Lin, H. Li, C. Wang, X. Xu, and M. Q.-H. Meng, "Hawkeye: Open source framework for field surveillance," in *2017 IEEE/RSJ International Conference on Intelligent Robots and Systems (IROS)*. IEEE, 2017, pp. 6083–6090.
- [3] K. Wada, E. Sucar, S. James, D. Lenton, and A. J. Davison, "Morefusion: Multi-object reasoning for 6d pose estimation from volumetric fusion," in *Proceedings of the IEEE/CVF Conference on Computer Vision and Pattern Recognition*, 2020, pp. 14 540–14 549.
- [4] E. Sucar, K. Wada, and A. Davison, "Neural object descriptors for multi-view shape reconstruction," *arXiv preprint arXiv:2004.04485*, 2020.
- [5] Y. Labbé, J. Carpentier, M. Aubry, and J. Sivic, "Cosypose: Consistent multi-view multi-object 6d pose estimation," *arXiv preprint arXiv:2008.08465*, 2020.
- [6] D. Almeida, E. Ataer-Cansizoglu, and R. Corcoran, "Detection, tracking and 3d modeling of objects with sparse rgb-d slam and interactive perception," in *2019 IEEE-RAS 19th International Conference on Humanoid Robots (Humanoids)*. IEEE, 2019, pp. 1–8.
- [7] Y. Wu, Y. Zhang, D. Zhu, Y. Feng, S. Coleman, and D. Kerr, "Eao-slam: Monocular semi-dense object slam based on ensemble data association," *arXiv preprint arXiv:2004.12730*, 2020.
- [8] Z. Zhang and D. Scaramuzza, "Beyond point clouds: Fisher information field for active visual localization," in *2019 International Conference on Robotics and Automation (ICRA)*. IEEE, 2019, pp. 5986–5992.
- [9] Z. Zeng, A. Röfer, and O. C. Jenkins, "Semantic linking maps for active visual object search," in *2020 IEEE International Conference on Robotics and Automation (ICRA)*. IEEE, 2020, pp. 1984–1990.
- [10] B. Charrow, G. Kahn, S. Patil, S. Liu, K. Goldberg, P. Abbeel, N. Michael, and V. Kumar, "Information-theoretic planning with trajectory optimization for dense 3d mapping," in *Robotics: Science and Systems*, vol. 11, 2015.
- [11] C. Wang, D. Zhu, T. Li, M. Q. Meng, and C. W. de Silva, "Efficient autonomous robotic exploration with semantic road map in indoor environments," *IEEE Robotics and Automation Letters*, vol. 4, no. 3, pp. 2989–2996, July 2019.
- [12] S. Kriegel, C. Rink, T. Bodenmüller, and M. Suppa, "Efficient next-best-scan planning for autonomous 3d surface reconstruction of unknown objects," *Journal of Real-Time Image Processing*, vol. 10, no. 4, pp. 611–631, 2015.
- [13] S. Yang and S. Scherer, "Cubeslam: Monocular 3-d object slam," *IEEE Transactions on Robotics*, vol. 35, no. 4, pp. 925–938, 2019.
- [14] G. Kahn, P. Sujaan, S. Patil, S. Bopardikar, J. Ryde, K. Goldberg, and P. Abbeel, "Active exploration using trajectory optimization for robotic grasping in the presence of occlusions," in *2015 IEEE International Conference on Robotics and Automation (ICRA)*. IEEE, 2015, pp. 4783–4790.
- [15] E. Arruda, J. Wyatt, and M. Kopicki, "Active vision for dexterous grasping of novel objects," in *2016 IEEE/RSJ International Conference on Intelligent Robots and Systems (IROS)*. IEEE, 2016, pp. 2881–2888.
- [16] A. Elfes, "Using occupancy grids for mobile robot perception and navigation," *Computer*, vol. 22, no. 6, pp. 46–57, 1989.
- [17] A. Tompkins, R. Senanayake, and F. Ramos, "Online domain adaptation for occupancy mapping," *arXiv preprint arXiv:2007.00164*, 2020.